Progress In Electromagnetics Research B, Vol. 6, 267–294, 2008

PLANE WAVE DIFFRACTION BY A FINITE PARALLEL-PLATE WAVEGUIDE WITH FOUR-LAYER MATERIAL LOADING: PART II — THE CASE OF H POLARIZATION

E. H. Shang and K. Kobayashi

Department of Electrical, Electronic, and Communication Engineering
Chuo University
Tokyo 112-8551, Japan

Abstract—The diffraction by a finite parallel-plate waveguide with four-layer material loading is rigorously analyzed by means of the Wiener-Hopf technique for the H-polarized plane wave incidence. Taking the Fourier transform for the unknown scattered field as well as the Helmholtz equation and applying boundary conditions in the transform domain, the problem is formulated in terms of the simultaneous Wiener-Hopf equations. The Wiener-Hopf equations are solved via the factorization and decomposition procedure together with the use of rigorous approximation procedures leading to an efficient approximation solution. The scattered field in the real space is evaluated explicitly by taking the inverse Fourier transform. Illustrative numerical examples on the radar cross section (RCS) are presented and the far field scattering characteristics of the waveguide are discussed.

1. INTRODUCTION

The analysis of the scattering from open-ended metallic waveguide cavities has received much attention from the viewpoints of electromagnetic theory as well as engineering applications such as radar technologies [1–4]. Cavity structures exist in many radar targets such as aircrafts and ships; therefore it is often required to reduce the radar cross section (RCS) either by loading the interior of cavities with absorbing materials or by shaping cavities. A number of diffraction problems involving two- and three-dimensional (2-D and 3-D) cavities have been analyzed thus far by means of high-frequency ray techniques and numerical methods [5–11]. The solutions obtained by these

approaches, however, may not be uniformly valid for arbitrary cavity dimensions. There are also important contributions to studies on the cavity RCS based on a rigorous function-theoretic approach due to the Wiener-Hopf technique [12, 13].

In the previous papers [14–17], we have carried out a rigorous RCS analysis of 2-D cavities with and without material loading, formed by a parallel-plate waveguide, using the Wiener-Hopf technique, where efficient approximate solutions valid over a broad frequency range have been obtained. Some of the important results on our RCS studies of several 2-D cavities are summarized in [18]. We have also considered a finite parallel-plate waveguide with three-layer material loading as a geometry that can form cavity structures, and carried out a rigorous Wiener-Hopf analysis of the plane wave diffraction [19, 20].

This paper is composed of two parts. We shall consider a finite parallel-plate waveguide with four-layer material loading as an important generalization to the geometry in [19, 20], and analyze the plane wave diffraction for both E and H polarizations rigorously by means of the Wiener-Hopf technique. In Part I [21] of this two-part paper, we have analyzed the case of E polarization, whereas in this second part, the H-polarized case will be considered. Introducing the Fourier transform for the unknown scattered field and applying boundary conditions in the transform domain, the problem is formulated in terms of the simultaneous Wiener-Hopf equations. The Wiener-Hopf equations are then solved via the factorization and decomposition procedure leading to the exact solution. This solution is, however, formal in the sense that it contains infinite series with unknown coefficients as well as infinite branch-cut integrals with unknown integrands. Employing a rigorous asymptotics, an approximate solution efficient for numerical computation is derived. Taking the inverse Fourier transform and using the saddle point method, a scattered field expression inside and outside the waveguide is explicitly evaluated. Representative numerical examples on the RCS are presented, and the far field scattering characteristics are discussed in detail. Some comparisons with the E-polarized case [21] will also be given. Since the method of solution employed here is similar to that in Part I, only the main results will be summarized.

The time factor is assumed to be $e^{-i\omega t}$, and suppressed throughout this paper.

2. FORMULATION OF THE PROBLEM

We consider the diffraction of an H-polarized plane wave by a finite parallel-plate waveguide with four-layer material loading, as shown

in Fig. 1, where the waveguide plates are infinitely thin, perfectly conducting, and uniform in the y-direction. The material layers I ($D_1 < z < D_2$), II ($D_2 < z < D_3$), III ($D_3 < z < D_4$), and IV ($D_4 < z < D_5$) are characterized by the relative permittivity/permeability (ε_m, μ_m) for $m = 1, 2, 3$, and 4, respectively.

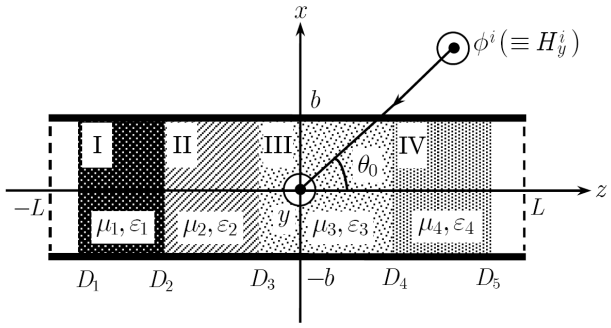

Figure 1. Geometry of the problem.

Let the total magnetic field $\phi^t(x,z)\left[\equiv H_y^t(x,z)\right]$ be

$$\phi^t(x,z) = \phi^i(x,z) + \phi(x,z), \tag{1}$$

where $\phi^i(x,z)$ is the incident field defined by

$$\phi^i(x,z) = e^{-ik(x\sin\theta_0 + z\cos\theta_0)},\ 0 < \theta_0 < \pi/2 \tag{2}$$

with $k\left[\equiv\ \omega(\varepsilon_0\mu_0)^{1/2}\right]$ being the free-space wavenumber. We shall assume that the vacuum is slightly lossy as in $k = k_1 + ik_2$ with $0 < k_2 \ll k_1$, and take the limit $k_2 \to +0$ at the end of analysis.

The total field $\phi^t(x,z)$ satisfies the 2-D Helmholtz equation

$$\left[\partial^2/\partial x^2 + \partial^2/\partial z^2 + \mu(x,z)\varepsilon(x,z)k^2\right]\phi^t(x,z) = 0, \tag{3}$$

where

$$\mu(x,z) = \begin{cases} \mu_1(\text{layer I}) \\ \mu_2(\text{layer II}) \\ \mu_3(\text{layer III}), \\ \mu_4(\text{layer IV}) \\ 1(\text{otherwise}) \end{cases} \quad \varepsilon(x,z) = \begin{cases} \varepsilon_1(\text{layer I}) \\ \varepsilon_2(\text{layer II}) \\ \varepsilon_3(\text{layer III}). \\ \varepsilon_4(\text{layer IV}) \\ 1(\text{otherwise}) \end{cases} \tag{4}$$

Once the solution of (3) has been determined, nonzero components of the total electromagnetic fields are derived from

$$\left(H_y^t, E_x^t, E_z^t\right) = \left[\phi^t, \frac{1}{i\omega\varepsilon_0\varepsilon(x,z)}\frac{\partial\phi^t}{\partial z}, \frac{i}{\omega\varepsilon_0\varepsilon(x,z)}\frac{\partial\phi^t}{\partial x}\right]. \tag{5}$$

Let us define the Fourier transform of the scattered field as

$$\Phi(x,\alpha) = (2\pi)^{-1/2}\int_{-\infty}^{\infty}\phi(x,z)e^{i\alpha z}dz,$$
$$\alpha = \mathrm{Re}\alpha + i\mathrm{Im}\alpha(\equiv \sigma + i\tau). \tag{6}$$

Introducing the Fourier integrals as

$$\Phi_{\pm}(x,\alpha) = \pm(2\pi)^{-1/2}\int_{\pm L}^{\pm\infty}\phi(x,z)e^{i\alpha(z\mp L)}dz, \tag{7}$$
$$\Phi_1(x,\alpha) = (2\pi)^{-1/2}\int_{-L}^{D_1}\phi^t(x,z)e^{i\alpha z}dz, \tag{8}$$
$$\Phi_m(x,\alpha) = (2\pi)^{-1/2}\int_{D_{m-1}}^{D_m}\phi^t(x,z)e^{i\alpha z}dz,\ m=2,3,4,5, \tag{9}$$
$$\Phi_6(x,\alpha) = (2\pi)^{-1/2}\int_{D_5}^{L}\phi^t(x,z)e^{i\alpha z}dz, \tag{10}$$

we can express $\Phi(x,\alpha)$ as

$$\Phi(x,\alpha) = \Psi(x,\alpha) + \sum_{m=1}^{6}\Phi_m(x,\alpha), \tag{11}$$

where

$$\Psi(x,\alpha) = e^{-i\alpha L}\Psi_-(x,\alpha) + e^{i\alpha L}\Psi_{(+)}(x,\alpha), \tag{12}$$
$$\Psi_-(x,\alpha) = \Phi_-(x,\alpha) + A\frac{e^{-ikx\sin\theta_0}}{\alpha - k\cos\theta_0}, \tag{13}$$
$$\Psi_{(+)}(x,\alpha) = \Phi_+(x,\alpha) - B\frac{e^{-ikx\sin\theta_0}}{\alpha - k\cos\theta_0}, \tag{14}$$
$$A = \frac{e^{ikL\cos\theta_0}}{(2\pi)^{1/2}i}, \quad B = \frac{e^{-ikL\cos\theta_0}}{(2\pi)^{1/2}i}. \tag{15}$$

Taking appropriate Fourier integrations and transforms of (3) and solving the resultant equations with the aid of the procedure similar to that employed in Part I [21], we obtain the scattered field representation in the Fourier transform domain as in

$$\Phi(x,\alpha) = \mp\gamma^{-1}\Psi'(\pm b,\alpha)e^{\mp\gamma(x\mp b)} \text{ for } x \gtrless \pm b,$$
$$= \Psi'(b,\alpha)\frac{\cosh\gamma(x+b)}{\gamma\sinh 2\gamma b} - \Psi'(-b,\alpha)\frac{\cosh\gamma(x-b)}{\gamma\sinh 2\gamma b}$$

$$-\frac{1}{b}\sum_{n=0}^{\infty}\delta_n\frac{e^{-i\alpha D_5}c_{5n}^{+}(\alpha)-e^{-i\alpha D_1}c_{1n}^{-}(\alpha)}{\alpha^2+\gamma_n^2}\cos\frac{n\pi}{2b}(x+b)$$
$$+\frac{1}{b}\sum_{m=1}^{4}\sum_{n=0}^{\infty}\delta_n\frac{e^{i\alpha D_m}c_{mn}^{+}(\alpha)-e^{i\alpha D_{m+1}}c_{m+1,n}^{-}(\alpha)}{\alpha^2+\Gamma_{mn}^2}$$
$$\cdot\cos\frac{n\pi}{2b}(x+b)\ \text{for}\ |x|<b, \tag{16}$$

where $\gamma=(\alpha^2-k^2)^{1/2}$ with $\mathrm{Re}\gamma>0$, and

$$\Psi'(\pm b,\alpha)=e^{-i\alpha L}\frac{U_{-}(\alpha)\pm V_{-}(\alpha)}{2}+e^{i\alpha L}\frac{U_{(+)}(\alpha)\pm V_{(+)}(\alpha)}{2}, \tag{17}$$
$$U_{-}(\alpha)=\Psi'_{-}(b,\alpha)+\Psi'_{-}(-b,\alpha), \tag{18}$$
$$U_{(+)}(\alpha)=\Psi'_{(+)}(b,\alpha)+\Psi'_{(+)}(-b,\alpha), \tag{19}$$
$$V_{-}(\alpha)=\Psi'_{-}(b,\alpha)-\Psi'_{-}(-b,\alpha), \tag{20}$$
$$V_{(+)}(\alpha)=\Psi'_{(+)}(b,\alpha)-\Psi'_{(+)}(-b,\alpha), \tag{21}$$
$$\delta_0=1/2;\ \delta_n=1\ \text{for}\ n\geq 1, \tag{22}$$
$$\gamma_0=-ik;\ \gamma_n=\left[(n\pi/2b)^2-k^2\right]^{1/2}\ \text{for}\, n\geq 1, \tag{23}$$
$$\Gamma_{m0}=-iK_m;\Gamma_{mn}=\left[(n\pi/2b)^2-K_m^2\right]^{1/2}\text{for}\ n\geq 1(m=1,2,3,4), \tag{24}$$
$$c_{1n}^{-}(\alpha)=\varepsilon_1^{-1}f_{1n}-i\alpha g_{1n}, c_{1n}^{+}(\alpha)=f_{1n}-i\alpha g_{1n}, \tag{25}$$
$$c_{2n}^{-}(\alpha)=(\varepsilon_1/\varepsilon_2)f_{2n}-i\alpha g_{2n}, c_{2n}^{+}(\alpha)=f_{2n}-i\alpha g_{2n}, \tag{26}$$
$$c_{3n}^{-}(\alpha)=f_{3n}-i\alpha g_{3n}, c_{3n}^{+}(\alpha)=(\varepsilon_3/\varepsilon_2)f_{3n}-i\alpha g_{3n}, \tag{27}$$
$$c_{4n}^{+}(\alpha)=f_{4n}-i\alpha g_{4n}, c_{4n}^{-}(\alpha)=f_{4n}-i\alpha g_{4n}, \tag{28}$$
$$c_{5n}^{-}(\alpha)=f_{5n}-i\alpha g_{5n}, c_{5n}^{+}(\alpha)=\varepsilon_4^{-1}f_{5n}-i\alpha g_{5n} \tag{29}$$

with $K_m=(\mu_m\varepsilon_m)^{1/2}k$. The prime in (17)–(21) implies differentiation with respect to x. The coefficients f_{mn} and g_{mn} for $m=1,2,3,4,5$ appearing in (25)–(29) are defined in Appendix.

Setting $x=b\pm 0$ and $x=-b\pm 0$ in (16) and taking into account the boundary conditions, we derive that

$$J_1^d(\alpha) = -\frac{e^{-i\alpha L}U_{-}(\alpha)+e^{i\alpha L}U_{(+)}(\alpha)}{M(\alpha)}$$
$$+\sum_{n=1,\,\mathrm{odd}}^{\infty}\frac{2}{b}\left[\frac{e^{i\alpha D_5}c_{5n}^{+}(\alpha)-e^{i\alpha D_1}c_{1n}^{-}(\alpha)}{\alpha^2+\gamma_n^2}\right.$$
$$\left.-\sum_{m=1}^{4}\frac{e^{i\alpha D_m}c_{mn}^{+}(\alpha)-e^{i\alpha D_{m+1}}c_{m+1,n}^{-}(\alpha)}{\alpha^2+\Gamma_{mn}^2}\right], \tag{30}$$

$$J_1^s(\alpha) = -\frac{e^{-i\alpha L}V_-(\alpha) + e^{i\alpha L}V_{(+)}(\alpha)}{N(\alpha)} - \sum_{n=0,\,\text{even}}^{\infty} \frac{2}{b}\delta_n \left[\frac{e^{i\alpha D_5}c_{5n}^+(\alpha) - e^{i\alpha D_1}c_{1n}^-(\alpha)}{\alpha^2+\gamma_n^2} - \sum_{m=1}^{4} \frac{e^{i\alpha D_m}c_{mn}^+(\alpha) - e^{i\alpha D_{m+1}}c_{m+1,n}^-(\alpha)}{\alpha^2+\Gamma_{mn}^2} \right], \quad (31)$$

where

$$J_1^{d,\,s}(\alpha) = J_1(b,\alpha) \mp J_1(-b,\alpha), \quad (32)$$

$$J_1(\pm b,\alpha) = \Phi_1(\pm b \pm 0,\alpha) - \Phi_1(\pm b \mp 0,\alpha), \quad (33)$$

$$M(\alpha) = \gamma e^{-\gamma b}\cosh\gamma b, \quad N(\alpha) = \gamma e^{-\gamma b}\sinh\gamma b. \quad (34)$$

Equations (30) and (31) are the desired simultaneous Wiener-Hopf equations satisfied by the unknown functions. In the next section, we will solve the Wiener-Hopf equations, and derive exact and approximate solutions.

3. SOLUTION OF THE WIENER-HOPF EQUATIONS

The kernel functions $M(\alpha)$ and $N(\alpha)$ given by (34) are factorized as [20]

$$M(\alpha) = M_+(\alpha)M_-(\alpha), N(\alpha) = N_+(\alpha)N_-(\alpha), \quad (35)$$

where

$$\begin{aligned} & M_+(\alpha)[= M_-(-\alpha)] \\ = \; & (\cos kb)^{1/2}e^{i3\pi/4}(k+\alpha)^{1/2}\exp\{(i\gamma b/\pi)\ln[(\alpha-\gamma)/k]\} \\ & \cdot\exp\{(i\alpha b/\pi)[1-C+\ln(\pi/2kb)+i\pi/2]\} \\ & \cdot\prod_{n=1,\,\text{odd}}^{\infty}(1+\alpha/i\gamma_n)e^{2i\alpha b/n\pi}, \end{aligned} \quad (36)$$

$$\begin{aligned} & N_+(\alpha)[= N_-(-\alpha)] \\ = \; & (k\sin kb)^{1/2}e^{i\pi/2}\exp\{(i\alpha b/\pi)\ln[(\alpha-\gamma)/k]\} \\ & \cdot\exp\{(i\alpha b/\pi)[1-C+\ln(2\pi/kb)+i\pi/2]\} \\ & \cdot(1+\alpha/i\gamma_0)\prod_{n=2,\,\text{even}}^{\infty}(1+\alpha/i\gamma_n)e^{2i\alpha b/n\pi} \end{aligned} \quad (37)$$

with $C(= 0.57721556\ldots)$ being Euler's constant. We multiply both sides of (30) and (31) by $e^{\pm i\alpha L}M_{\pm}(\alpha)$ and $e^{\pm i\alpha L}N_{\pm}(\alpha)$, respectively, and apply the decomposition procedure. Omitting the details, we obtain that

$$\begin{aligned} U_{-}(\alpha) &= b^{1/2}M_{-}(\alpha)\left[-\frac{A_u}{b\left(\alpha-k\cos\theta_0\right)}+\frac{J_u^{(1)}(\alpha)}{b^{1/2}}\right. \\ &\quad +\sum_{n=2}^{\infty}\frac{e^{-2\gamma_{2n-3}(L+D_1)}X_{2n-3}^{-}a_np_nu_n^{-}}{b\left(\alpha-i\gamma_{2n-3}\right)} \\ &\quad \left.+\sum_{n=2}^{\infty}\frac{e^{-\gamma_{2n-3}(2L+D_1-D_5)}Y_{2n-3}^{-}a_np_nu_n^{+}}{b\left(\alpha-i\gamma_{2n-3}\right)}\right], \end{aligned} \tag{38}$$

$$\begin{aligned} U_{(+)}(\alpha) &= b^{1/2}M_{+}(\alpha)\left[\frac{B_u}{b\left(\alpha-k\cos\theta_0\right)}+\frac{J_u^{(2)}(\alpha)}{b^{1/2}}\right. \\ &\quad -\sum_{n=2}^{\infty}\frac{e^{-2\gamma_{2n-3}(L-D_5)}X_{2n-3}^{+}a_np_nu_n^{+}}{b\left(\alpha+i\gamma_{2n-3}\right)} \\ &\quad \left.-\sum_{n=2}^{\infty}\frac{e^{-\gamma_{2n-3}(2L+D_1-D_5)}Y_{2n-3}^{+}a_np_nu_n^{-}}{b\left(\alpha+i\gamma_{2n-3}\right)}\right], \end{aligned} \tag{39}$$

$$\begin{aligned} V_{-}(\alpha) &= b^{1/2}N_{-}(\alpha)\left[-\frac{A_v}{b\left(\alpha-k\cos\theta_0\right)}+\frac{J_v^{(1)}(\alpha)}{b^{1/2}}\right. \\ &\quad +\sum_{n=1}^{\infty}\frac{\delta_{2n-2}e^{-2\gamma_{2n-2}(L+D_1)}X_{2n-2}^{-}b_nq_nv_n^{-}}{b\left(\alpha-i\gamma_{2n-2}\right)} \\ &\quad \left.+\sum_{n=1}^{\infty}\frac{\delta_{2n-2}e^{-\gamma_{2n-2}(2L+D_1-D_5)}Y_{2n-2}^{-}b_nq_nv_n^{+}}{b\left(\alpha-i\gamma_{2n-2}\right)}\right], \end{aligned} \tag{40}$$

$$\begin{aligned} V_{(+)}(\alpha) &= b^{1/2}N_{+}(\alpha)\left[\frac{B_v}{b\left(\alpha-k\cos\theta_0\right)}+\frac{J_v^{(2)}(\alpha)}{b^{1/2}}\right. \\ &\quad -\sum_{n=1}^{\infty}\frac{\delta_{2n-2}e^{-2\gamma_{2n-2}(L-D_5)}X_{2n-2}^{+}b_nq_nv_n^{+}}{b\left(\alpha+i\gamma_{2n-2}\right)} \\ &\quad \left.-\sum_{n=1}^{\infty}\frac{\delta_{2n-2}e^{-\gamma_{2n-2}(2L+D_1-D_5)}Y_{2n-2}^{+}b_nq_nv_n^{-}}{b\left(\alpha+i\gamma_{2n-2}\right)}\right], \end{aligned} \tag{41}$$

where

$$a_1 = (bi\gamma_0)^{-1};\ a_n = (bi\gamma_{2n-3})^{-1} \text{ for } n \geq 2, \tag{42}$$

$$b_1 = (bi\gamma_0)^{-1};\ b_n = (bi\gamma_{2n-2})^{-1} \text{ for } n \geq 2, \tag{43}$$

$$p_1 = b^{1/2}M_+(i\gamma_0);\ p_n = b^{1/2}M_+(i\gamma_{2n-3}) \text{ for } n \geq 2, \tag{44}$$

$$q_1 = b^{1/2}N_+(i\gamma_0);\ q_n = b^{1/2}N_+(i\gamma_{2n-2}) \text{ for } n \geq 2, \tag{45}$$

$$u_1^- = U_-(-i\gamma_0);\ u_n^- = b^{-1}U_-(-i\gamma_{2n-3}) \text{ for } n \geq 2, \tag{46}$$

$$u_1^+ = U_{(+)}(i\gamma_0);\ u_n^+ = b^{-1}U_{(+)}(i\gamma_{2n-3}) \text{ for } n \geq 2, \tag{47}$$

$$v_1^- = V_-(-i\gamma_0);\ v_n^- = b^{-1}V_-(-i\gamma_{2n-2}) \text{ for } n \geq 2, \tag{48}$$

$$v_1^+ = V_{(+)}(i\gamma_0);\ v_n^+ = b^{-1}V_{(+)}(i\gamma_{2n-2}) \text{ for } n \geq 2, \tag{49}$$

$$A_u = \frac{2A'\cos(kb\sin\theta_0)}{b^{1/2}M_-(k\cos\theta_0)}, \quad B_u = \frac{2B'\cos(kb\sin\theta_0)}{b^{1/2}M_+(k\cos\theta_0)}, \tag{50}$$

$$A_v = \frac{2iA'\sin(kb\sin\theta_0)}{b^{1/2}N_-(k\cos\theta_0)}, \quad B_v = \frac{2iB'\sin(kb\sin\theta_0)}{b^{1/2}N_+(k\cos\theta_0)}, \tag{51}$$

$$A' = -\frac{kb\sin\theta_0 e^{ikL\cos\theta_0}}{(2\pi)^{1/2}},\ B' = -\frac{kb\sin\theta_0 e^{-ikL\cos\theta_0}}{(2\pi)^{1/2}}, \tag{52}$$

$$J_u^{(1)}(\alpha) = \frac{1}{\pi i}\int_k^{k+i\infty} e^{2i\beta L}\frac{M_+(\beta)U_{(+)}(\beta)}{(\beta^2-k^2)^{1/2}(\beta-\alpha)}d\beta, \tag{53}$$

$$J_u^{(2)}(\alpha) = \frac{1}{\pi i}\int_k^{k+i\infty} e^{2i\beta L}\frac{M_+(\beta)U_-(-\beta)}{(\beta^2-k^2)^{1/2}(\beta+\alpha)}d\beta, \tag{54}$$

$$J_v^{(1)}(\alpha) = \frac{1}{\pi i}\int_k^{k+i\infty} e^{2i\beta L}\frac{N_+(\beta)V_{(+)}(\beta)}{(\beta^2-k^2)^{1/2}(\beta-\alpha)}d\beta, \tag{55}$$

$$J_v^{(2)}(\alpha) = \frac{1}{\pi i}\int_k^{k+i\infty} e^{2i\beta L}\frac{N_+(\beta)V_-(-\beta)}{(\beta^2-k^2)^{1/2}(\beta+\alpha)}d\beta. \tag{56}$$

Equations (38), (39) and (40), (41) are the exact solutions of the Wiener-Hopf Equations (30) and (31), respectively, but they are formal since the infinite series with the unknown coefficients $u_n^{\pm}(n = 2, 3, 4, \dots)$ and $v_n^{\pm}(n = 1, 2, 3, \dots)$ as well as the branch-cut integrals $J_u^{(1),(2)}(\alpha)$ and $J_v^{(1),(2)}(\alpha)$ with the unknown integrands $U_-(\alpha)$, $U_{(+)}(\alpha), V_-(\alpha)$, and $V_{(+)}(\alpha)$ are involved. Applying a rigorous asymptotics similar to that employed for the E-polarized case [21], an approximate solution efficient for numerical computation can be

obtained as follows:

$$
\begin{aligned}
U_{-}(\alpha) \approx b^{1/2} M_{-}(\alpha) \Bigg(& \frac{A_u}{b\left(\alpha - k\cos\theta_0\right)} \\
& + a_1 p_1 \left\{ \left[u_1^{+} + \frac{2B' \cos\left(kb\sin\theta_0\right)}{kb\left(1-\cos\theta_0\right)} \right] \xi(-\alpha) \right. \\
& \left. + \frac{2B'L}{b} \cos\left(kb\sin\theta_0\right) \frac{\xi(-\alpha) - \xi(-k\cos\theta_0)}{(-\alpha + k\cos\theta_0)L} \right\} \\
& + \sum_{n=2}^{N-1} \frac{a_n p_n X_{2n-3}^{-} e^{-2\gamma_{2n-3}(L+D_1)} u_n^{-}}{b\left(\alpha - i\gamma_{2n-3}\right)} \\
& + \sum_{n=2}^{N-1} \frac{a_n p_n Y_{2n-3}^{-} e^{-\gamma_{2n-3}(2L+D_1-D_5)} u_n^{+}}{b\left(\alpha - i\gamma_{2n-3}\right)} \\
& + K_u^{(1)} \sum_{n=N}^{\infty} \frac{e^{-2\gamma_{2n-3}(L+D_1)} X_{2n-3}^{-} \left(b\gamma_{2n-3}\right)^{-1}}{b\left(\alpha - i\gamma_{2n-3}\right)} \\
& + K_u^{(2)} \sum_{n=N}^{\infty} \frac{e^{-\gamma_{2n-3}(2L+D_1-D_5)} Y_{2n-3}^{-} \left(b\gamma_{2n-3}\right)^{-1}}{b\left(\alpha - i\gamma_{2n-3}\right)} \Bigg), \quad (57)
\end{aligned}
$$

$$
\begin{aligned}
U_{(+)}(\alpha) \approx b^{1/2} M_{+}(\alpha) \Bigg(& -\frac{B_u}{b\left(\alpha - k\cos\theta_0\right)} \\
& + a_1 p_1 \left\{ \left[u_1^{-} + \frac{2A' \cos\left(kb\sin\theta_0\right)}{kb\left(1+\cos\theta_0\right)} \right] \xi(\alpha) \right. \\
& \left. + \frac{2A'L}{b} \cos\left(kb\sin\theta_0\right) \frac{\xi(\alpha) - \xi(k\cos\theta_0)}{(\alpha - k\cos\theta_0)L} \right\} \\
& - \sum_{n=2}^{N-1} \frac{a_n p_n X_{2n-3}^{+} e^{-2\gamma_{2n-3}(L-D_5)} u_n^{+}}{b\left(\alpha + i\gamma_{2n-3}\right)} \\
& - \sum_{n=2}^{N-1} \frac{a_n p_n Y_{2n-3}^{+} e^{-\gamma_{2n-3}(2L+D_1-D_5)} u_n^{-}}{b\left(\alpha + i\gamma_{2n-3}\right)} \\
& - K_u^{(1)} \sum_{n=N}^{\infty} \frac{e^{-2\gamma_{2n-3}(L-D_5)} X_{2n-3}^{+} \left(b\gamma_{2n-3}\right)^{-1}}{b\left(\alpha + i\gamma_{2n-3}\right)} \\
& - K_u^{(2)} \sum_{n=N}^{\infty} \frac{e^{-\gamma_{2n-3}(2L+D_1-D_5)} Y_{2n-3}^{+} \left(b\gamma_{2n-3}\right)^{-1}}{b\left(\alpha + i\gamma_{2n-3}\right)} \Bigg), \quad (58)
\end{aligned}
$$

$$
\begin{aligned}
V_{-}(\alpha) \approx\, & b^{1/2} N_{-}(\alpha) \left(-\frac{A_v}{b\,(\alpha - k\cos\theta_0)} \right. \\
& + b_1 q_1 \left\{ \left[v_1^{+} - \frac{2iB' \sin\left(kb\sin\theta_0\right)}{kb\,(1-\cos\theta_0)} \right] \xi(-\alpha) \right. \\
& \left. - \frac{2iB'L}{b} \sin\left(kb\sin\theta_0\right) \frac{\xi(-\alpha) - \xi(-k\cos\theta_0)}{(-\alpha + k\cos\theta_0)L} \right\} \\
& + \sum_{n=1}^{N-1} \frac{\delta_{2n-2} b_n q_n X_{2n-2}^{-} e^{-2\gamma_{2n-2}(L+D_1)} v_n^{-}}{b\,(\alpha - i\gamma_{2n-2})} \\
& + \sum_{n=1}^{N-1} \frac{\delta_{2n-2} b_n q_n Y_{2n-2}^{-} e^{-\gamma_{2n-2}(2L+D_1-D_5)} v_n^{+}}{b\,(\alpha - i\gamma_{2n-2})} \\
& + K_v^{(1)} \sum_{n=N}^{\infty} \frac{e^{-2\gamma_{2n-2}(L+D_1)} X_{2n-2}^{-} \left(b\gamma_{2n-2}\right)^{-1}}{b\,(\alpha - i\gamma_{2n-2})} \\
& \left. + K_v^{(2)} \sum_{n=N}^{\infty} \frac{e^{-\gamma_{2n-2}(2L+D_1-D_5)} Y_{2n-2}^{-} \left(b\gamma_{2n-2}\right)^{-1}}{b\,(\alpha - i\gamma_{2n-2})} \right), \qquad (59)
\end{aligned}
$$

$$
\begin{aligned}
V_{(+)}(\alpha) \approx\, & b^{1/2} N_{+}(\alpha) \left(\frac{B_v}{b\,(\alpha - k\cos\theta_0)} \right. \\
& + b_1 q_1 \left\{ \left[v_1^{-} - \frac{2iA' \sin\left(kb\sin\theta_0\right)}{kb\,(1+\cos\theta_0)} \right] \xi(\alpha) \right. \\
& \left. - \frac{2iA'L}{b} \sin\left(kb\sin\theta_0\right) \frac{\xi(\alpha) - \xi(k\cos\theta_0)}{(\alpha - k\cos\theta_0)L} \right\} \\
& - \sum_{n=1}^{N-1} \frac{\delta_{2n-2} b_n q_n X_{2n-2}^{+} e^{-2\gamma_{2n-2}(L-D_5)} v_n^{+}}{b\,(\alpha + i\gamma_{2n-2})} \\
& - \sum_{n=1}^{N-1} \frac{\delta_{2n-2} b_n q_n Y_{2n-2}^{+} e^{-\gamma_{2n-2}(2L+D_1-D_5)} v_n^{-}}{b\,(\alpha + i\gamma_{2n-2})} \\
& - K_v^{(1)} \sum_{n=N}^{\infty} \frac{e^{-2\gamma_{2n-2}(L-D_5)} X_{2n-2}^{+} \left(b\gamma_{2n-2}\right)^{-1}}{b\,(\alpha + i\gamma_{2n-2})} \\
& \left. - K_v^{(2)} \sum_{n=N}^{\infty} \frac{e^{-\gamma_{2n-2}(2L+D_1-D_5)} Y_{2n-2}^{+} \left(b\gamma_{2n-2}\right)^{-1}}{b\,(\alpha + i\gamma_{2n-2})} \right), \qquad (60)
\end{aligned}
$$

where

$$\xi(\alpha) = \frac{(kL)^{1/2} e^{i(2kL-3\pi/4)}}{\pi} \Gamma_1 \left[1/2,\, -2i(\alpha+k)L\right], \tag{61}$$

In (61), $\Gamma_1(\cdot,\cdot)$ is the generalized gamma function [22] defined by

$$\Gamma_m(u,v) = \int_0^\infty \frac{t^{u-1}e^{-t}}{(t+v)^m} dt \tag{62}$$

for $\mathrm{Re}u > 0$, $|v| > 0$, $|\arg v| < \pi$, and positive integer m. In the derivation of (57)–(60), it has been taken into account that, in view of the edge condition, the unknowns $u_n^{\pm}(n = 2,3,4,\dots)$, and $v_n^{\pm}(n = 1,2,3,\dots)$ defined by (47) and (48) show the asymptotic behavior

$$u_n^- \sim -2^{1/2} i K_u^{(1)} \left(b\gamma_{2n-3}\right)^{-1/2}, u_n^+ \sim -2^{1/2} i K_u^{(2)} \left(b\gamma_{2n-3}\right)^{-1/2}, \tag{63}$$

$$v_n^- \sim -2^{1/2} i K_v^{(1)} \left(b\gamma_{2n-2}\right)^{-1/2}, v_n^+ \sim -2^{1/2} i K_v^{(2)} \left(b\gamma_{2n-2}\right)^{-1/2} \tag{64}$$

as $n \to \infty$.

Equations (57), (58) and (59), (60) are approximate solutions of the Wiener-Hopf Equations (30) and (31), respectively, which are valid for large positive integer N and large $|k|\,L$. The unknown $u_n^{\pm}$ and $v_n^{\pm}$ for $n = 1,2,\dots,N-1$ and $K_u^{(1),(2)}, K_v^{(1),(2)}$ are involved in (57)–(60), which can be determined with high accuracy by solving appropriate $2N \times 2N$ matrix equations numerically.

4. SCATTERED FIELD

The scattered field can be derived by taking the inverse Fourier transform of (16) in accordance with

$$\phi(x,z) = (2\pi)^{-1/2} \int_{-\infty+ic}^{\infty+ic} \Phi(x,\alpha) e^{-i\alpha z} d\alpha,\ |c| < k_2 \cos\theta_0. \tag{65}$$

After some manipulations, an explicit expression for the total field inside the waveguide is found to be

$$\begin{aligned}
\phi^t(x,z) &= \sum_{n=0}^{\infty} \left[T_{Ln}^+ e^{\gamma_n(z-D_1)} - T_{Ln}^- e^{-\gamma_n(z-D_1)}\right] \cos\frac{n\pi}{2b}(x+b) \\
&\qquad \text{for} - L < z < D_1, \\
&= \sum_{m=1}^{4} \sum_{n=0}^{\infty} \left[T_{mn}^+ e^{\Gamma_m(z-D_m)} - T_{mn}^- e^{-\Gamma_m(z-D_m)}\right] \cos\frac{n\pi}{2b}(x+b) \\
&\qquad \text{for } D_m < z < D_{m+1} (m = 1,2,3,4),
\end{aligned}$$

$$= \sum_{n=0}^{\infty} [T_{Rn}^{+} e^{\gamma_n (z-D_5)} - T_{Rn}^{-} e^{-\gamma_n (z-D_5)}] \cos \frac{n\pi}{2b}(x+b)$$
$$\text{for } D_5 < z < L, \tag{66}$$

where

$$T_{Ln}^{-} = \kappa_n e^{-\gamma_n (L+D_1)} U_{-}(-i\gamma_n) \text{ for odd } n,$$
$$= -\kappa_n e^{-\gamma_n (L+D_1)} V_{-}(-i\gamma_n) \text{ for even } n, \tag{67}$$
$$T_{Ln}^{+} = \kappa_n \left[X_n^{-} e^{-\gamma_n (L+D_1)} U_{-}(-i\gamma_n) \right.$$
$$\left. \cdot Y_n^{-} e^{-\gamma_n (L-D_5)} U_{(+)}(i\gamma_n) \right] \text{ for odd } n,$$
$$= -\kappa_n \left[X_n^{-} e^{-\gamma_n (L+D_1)} V_{-}(-i\gamma_n) \right.$$
$$\left. \cdot Y_n^{-} e^{-\gamma_n (L-D_5)} V_{(+)}(i\gamma_n) \right] \text{ for even } n, \tag{68}$$
$$T_{Rn}^{-} = -\chi_n \left[Y_n^{+} e^{-\gamma_n (L+D_1)} U_{-}(-i\gamma_n) \right.$$
$$\left. \cdot X_n^{-} e^{-\gamma_n (L-D_5)} U_{(+)}(i\gamma_n) \right] \text{ for odd } n,$$
$$= \chi_n \left[Y_n^{+} e^{-\gamma_n (L+D_1)} V_{-}(-i\gamma_n) \right.$$
$$\left. \cdot X_n^{-} e^{-\gamma_n (L-D_5)} V_{(+)}(i\gamma_n) \right] \text{ for even } n, \tag{69}$$
$$T_{Rn}^{+} = -\chi_n e^{-\gamma_n (L-D_5)} U_{(+)}(i\gamma_n) \text{ for odd } n,$$
$$= \chi_n e^{-\gamma_n (L-D_5)} V_{(+)}(i\gamma_n) \text{ for even } n, \tag{70}$$
$$T_{mn}^{-} = K_{mn} \left[R_{mn}^{-} U_{-}(-i\gamma_n) + S_{mn}^{-} U_{(+)}(i\gamma_n) \right]$$
$$\text{for odd } n \, (m = 1, 2, 3, \, 4),$$
$$= -K_{mn} \left[R_{mn}^{-} V_{-}(-i\gamma_n) + S_{mn}^{-} V_{(+)}(i\gamma_n) \right]$$
$$\text{for even } n \, (m = 1, 2, 3, \, 4), \tag{71}$$
$$T_{mn}^{+} = K_{mn} \left[R_{mn}^{+} U_{-}(-i\gamma_n) + S_{mn}^{+} U_{(+)}(i\gamma_n) \right]$$
$$\text{for odd } n \, (m = 1, 2, 3, 4),$$
$$= -K_{mn} \left[R_{mn}^{+} V_{-}(-i\gamma_n) + S_{mn}^{+} V_{(+)}(i\gamma_n) \right]$$
$$\text{for even } n \, (m = 1, 2, 3, \, 4), \tag{72}$$
$$R_{1n}^{-} = P_{1n} - \Gamma_{1n} R_{1n}, R_{1n}^{+} = (\varepsilon_1/\varepsilon_2) P_{2n} + \Gamma_{1n} R_{2n}, \tag{73}$$
$$S_{1n}^{-} = Q_{1n} - \Gamma_{1n} S_{1n}, S_{1n}^{+} = (\varepsilon_1/\varepsilon_2) Q_{2n} + \Gamma_{1n} S_{2n}, \tag{74}$$
$$R_{2n}^{-} = P_{2n} - \Gamma_{2n} R_{2n}, R_{2n}^{+} = P_{3n} + \Gamma_{2n} R_{3n}, \tag{75}$$
$$S_{2n}^{-} = Q_{2n} - \Gamma_{2n} S_{2n}, S_{2n}^{+} = Q_{3n} + \Gamma_{2n} S_{3n}, \tag{76}$$

$$R_{3n}^{-}=(\varepsilon_3/\varepsilon_2)P_{3n}-\Gamma_{3n}R_{3n}, R_{3n}^{+}=P_{4n}+\Gamma_{3n}R_{4n}, \quad (77)$$

$$S_{3n}^{-}=(\varepsilon_3/\varepsilon_2)Q_{3n}-\Gamma_{3n}S_{3n}, S_{3n}^{+}=Q_{4n}+\Gamma_{3n}S_{4n}, \quad (78)$$

$$\kappa_n=\left(\frac{\pi}{2}\right)^{1/2}\frac{n\pi}{2b^2\gamma_n}; K_{mn}=\left(\frac{\pi}{2}\right)^{1/2}\frac{n\pi}{2b^2\Gamma_{mn}} \text{ for } m=1,2,3,4. \quad (79)$$

The coefficients P_{mn}, Q_{mn}, R_{mn}, and S_{mn} in (73)–(78) are defined in Appendix.

Using the field representation for $|x| > b$ in (16) and evaluating its inverse Fourier transform asymptotically with the aid of the saddle point method, the scattered far field is found to be

$$\phi(\rho,\theta)\sim\pm\Psi'(\pm b,-k\cos\theta_0)e^{\mp ikb\sin\theta_0}\frac{e^{i(k\rho-3\pi/4)}}{(k\rho)^{1/2}},\ x\gtrless\pm b \quad (80)$$

as $k\rho\to\infty$, where (ρ,θ) is the cylindrical coordinate defined by $x=\rho\sin\theta, z=\rho\cos\theta$ for $0<|\theta|<\pi$.

5. NUMERICAL RESULTS AND DISCUSSION

In this section, we shall present illustrative numerical examples of the RCS and discuss the far field scattering characteristics of the waveguide in detail. Numerical results presented below are based on the scattered far field expression given by (80) together with (17). We have used the approximate expressions as derived in (57)–(60) for computing $U_{-}(\alpha), U_{(+)}(\alpha), V_{-}(\alpha)$, and $V_{(+)}(\alpha)$ involved in (17). Since we treat the 2-D scattering problem, the RCS per unit length is given by

$$\sigma=\lim_{\rho\to\infty}\left(2\pi\rho|\phi|^2/|\phi^i|^2\right), \quad (81)$$

which reduces by using (80) to

$$\sigma=\lambda|\Psi'(\pm b,-k\cos\theta)|^2,\quad \theta\gtrless 0 \quad (82)$$

with λ being the free-space wavelength.

Figures 2, 3 and 4, 5 show numerical results of the monostatic RCS versus the incidence angle θ_0 and the bistatic RCS versus the observation angle θ, respectively, where the values of σ/λ are plotted in decibels [dB] by computing $10\log_{10}\sigma/\lambda$. In the bistatic RCS, the incidence angle has been fixed as $\theta_0=45^\circ$ for numerical computation. In order to enable comparison between different polarizations, we have chosen the same parameters as in the E-polarized case analyzed in Part I [21]. The normalized waveguide aperture width and the waveguide dimension ratio are taken as $kb = 3.14, 15.7, 31.4$, and

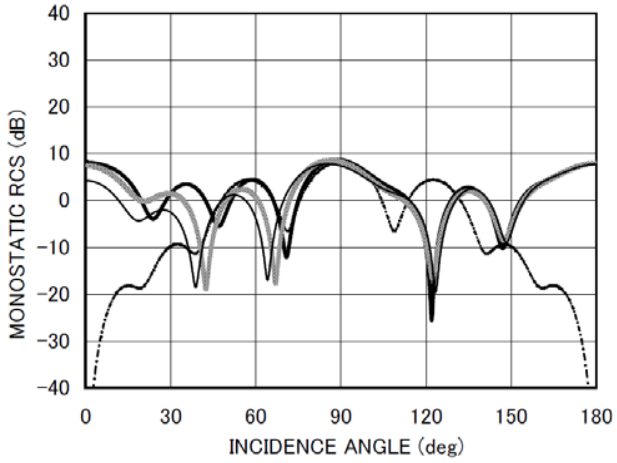

Figure 2a. Monostatic RCS σ/λ [dB] for $L/b = 1.0, kb = 3.14$. -·-·-·-·-·- empty waveguide (layers I-IV: vacuum). ——: cavity with no loading (layer I: perfect conductor; layers II-IV: vacuum; $t_L = 0.6\,L,\ t_{\rm PEC} = 0.4L,\ t_R = L$). ——: cavity with two-layer loading (layer I: perfect conductor; layer II: $\varepsilon_2 = 3.14 + i10.0,\ \mu_2 = 1.0$; layer III: $\varepsilon_3 = 1.6 + i0.9,\ \mu_3 = 1.0$; layer IV: vacuum; $t_L = 0.6L,\ t_{\rm PEC} = 0.4L,\ t_R = L,\ t_{\rm 2layer} = 0.4L$). ——: cavity with three-layer loading (layer I: perfect conductor; layers II-IV: Emerson & Cuming AN-73; $t_L = 0.6L,\ t_{\rm PEC} = 0.4L,\ t_R = L,\ t_{\rm 3layer} = 0.6L$).

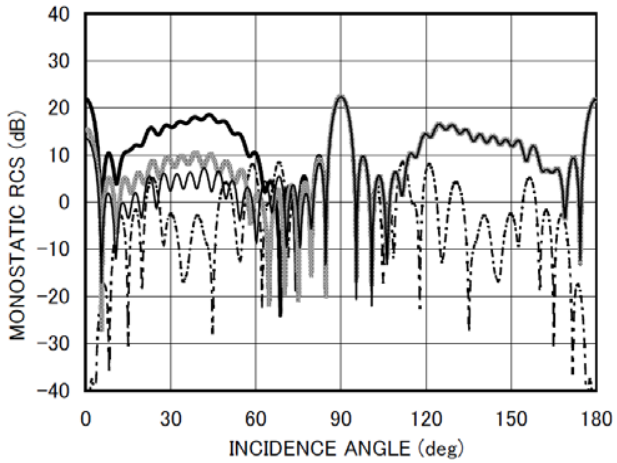

Figure 2b. Monostatic RCS $\sigma/\lambda\,[\,{\rm dB}]$ for $L/b = 1.0, kb = 15.7$. Other particulars are the same as in Fig. 2a.

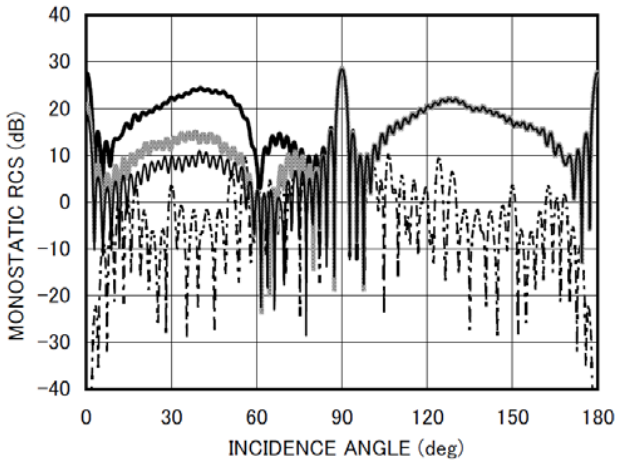

Figure 2c. Monostatic RCS $\sigma/\lambda\,[\,\mathrm{dB}]$ for $L/b = 1.0, kb = 31.4$. Other particulars are the same as in Fig. 2a.

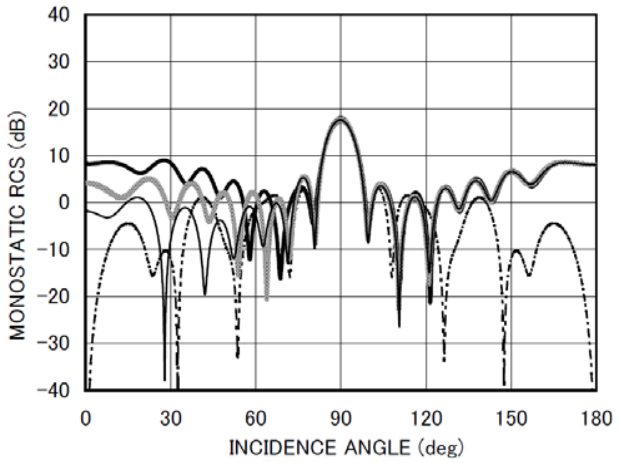

Figure 3a. Monostatic RCS $\sigma/\lambda\,[\,\mathrm{dB}]$ for $L/b = 3.0,\ kb = 3.14$. Other particulars are the same as in Fig. 2a.

$L/b = 1.0, 3.0$, respectively. By choosing layer I as perfect conductors, we have formed the two cavities at the left ($-L < z < D_1$) and right ($D_2 < z < L$) sides of the waveguide. We have fixed the cavity depth as $t_L(= D_1 + L) = 0.6L$ and $t_R(= L - D_2) = L$ for the left and right cavities, respectively, and the thickness of perfect conductors (layer I) has been chosen as $t_{\mathrm{PEC}}(= D_2 - D_1) = 0.4L$. In order

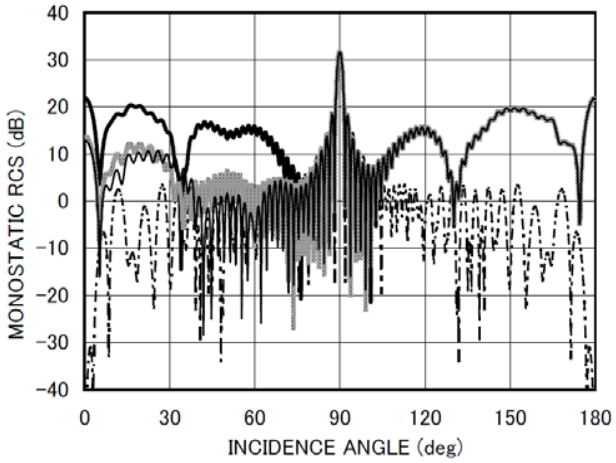

Figure 3b. Monostatic RCS σ/λ [dB] for $L/b = 3.0,\ kb = 15.7$. Other particulars are the same as in Fig. 2a.

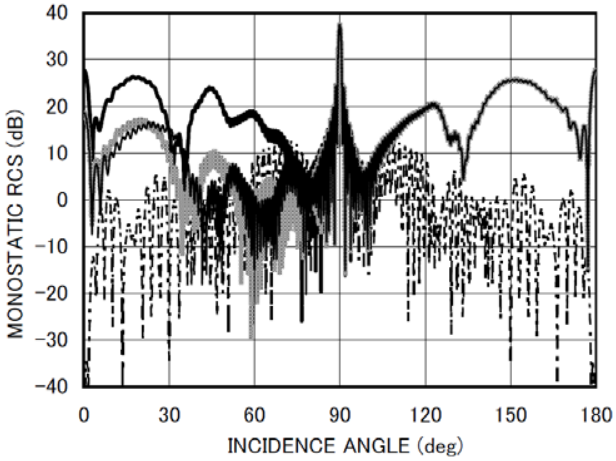

Figure 3c. Monostatic RCS σ/λ [dB] for $L/b = 3.0,\ kb = 31.4$. Other particulars are the same as in Fig. 2a.

to investigate the RCS reduction effect, numerical computation has been carried out for the three different cavity geometries, namely, an empty cavity with layers II-IV being vacuum and the case where the two- and three-layer materials are loaded in the right cavity. As an example of existing three-layer materials, Emerson & Cuming AN-73 has been chosen in numerical computation, where the material

parameters in layers II–IV are $\varepsilon_{r2} = 3.14 + i10.0$, $\mu_{r2} = 1.0$, $\varepsilon_{r3} = 1.6 + i0.9$, $\mu_{r3} = 1.0$, $\varepsilon_{r4} = 1.4 + i0.35$, $\mu_{r4} = 1.0$, and the layer thickness is such that $D_3 - D_2 = D_4 - D_3 = D_5 - D_4 (= t_{3\text{layer}}/3)$. We have also computed the cavity RCS for the two-layer material loading, where $\varepsilon_{r2} = 3.14 + i10.0$, $\mu_{r2} = 1.0$, $\varepsilon_{r3} = 1.6 + i0.9$, $\mu_{r3} = 1.0$, $\varepsilon_{r4} = \mu_{r4} = 1.0$, and $D_3 - D_2 = D_4 - D_3 (= t_{2\text{layer}}/2)$. This two-layer material loading is the case where layer IV of Emerson & Cuming AN-73 has been removed. The thickness of the two- and three-layer materials is chosen as $t_{2\text{layer}} = 0.4L$ and $t_{3\text{layer}} = 0.6L$, respectively. The results for the parallel-plate waveguide with no material loading (layers I-IV are vacuum) have also been added for comparison.

From Figs. 2 and 3, we see that, as in the E-polarized case [21], the monostatic RCS for the empty cavity shows noticeable peaks at $\theta_0 = 0^\circ, 90^\circ, 180^\circ$ in all examples which are due to the specular reflection from the upper plate at $x = b$ and the internal plates at $z = D_1, D_2$ of the waveguide. The RCS at $\theta_0 = 0^\circ$ is reduced for the case of material loading inside the right cavity as expected. The other common feature between the E and H polarizations is that, the RCS characteristics for empty and loaded cavities are nearly identical to each other over the range $90^\circ \leq \theta_0 \leq 180^\circ$, whereas there are great differences in the scattering characteristics over the range $0^\circ \leq \theta_0 \leq 90^\circ$ depending on materials inside the right cavity. It is therefore confirmed that the differences in the material inside the right cavity affects the backscattering only for the region ($0^\circ \leq \theta_0 \leq 90^\circ$) where the aperture of the right cavity is visible from the incident direction. Similarly we see that, for the region $90^\circ \leq \theta_0 \leq 180^\circ$, only the left cavity (no material loading) is visible from the incident direction and hence, structural differences in the interior of the right cavity do not contribute to the monostatic far field scattering.

Next we shall investigate the RCS reduction characteristics by comparing the RCS results for empty and loaded cavities. It is seen from Figs. 2 and 3 that, for cavities of $kb = 15.7, 31.4$ with no material loading, the monostatic RCS exhibits fairly large values for $0^\circ \leq \theta_0 \leq 70^\circ$ and $110^\circ \leq \theta_0 \leq 180^\circ$ due to the interior irradiation from both the left and right cavities, whereas the irradiation for the range $0^\circ \leq \theta_0 \leq 70^\circ$ is reduced for the case of material loading in the right cavity. We also observe that this RCS reduction is noticeable for larger cavities. By comparing the characteristics for the two-layer case with those for the three-layer case, it is found that the RCS reduction is more significant in the three-layer case. From these characteristics, it is inferred that the multi-layer loading gives rise to better RCS reduction over a broad frequency range.

Let us now make comparisons of the monostatic RCS results for

the H polarization in this paper with those for the E polarization analyzed in Part I [21], and investigate the differences on the backscattering characteristics depending on the incident polarization. Comparing the RCS curves in Figs. 2 and 3 for the H polarization with those in Figs. 3 and 4 in Part I for the E polarization, we see differences in all numerical examples. In particular, the monostatic RCS for the H polarization oscillates rapidly in comparison to the E-polarized case. This difference is due to the fact that the effect of edge diffraction depends on the incident polarization. We also see that, if the cavity aperture opening is small as in $kb = 3.14$, there are great differences in the RCS characteristics between the H polarization (Figs. 2(a) and 3(a) in this paper) and the E polarization (Figs. 3(a) and 4(a) in Part I) except in the neighborhood of the main lobe direction $\theta_0 = 90°$. This is because the diffraction phenomena at low frequencies strongly depend on the incident polarization. It is also found that, with an increase of the cavity opening, the RCS exhibits close features for both polarizations.

Figures 4 and 5 show numerical examples of the bistatic RCS as a function of observation angle θ, where the incidence angle is fixed

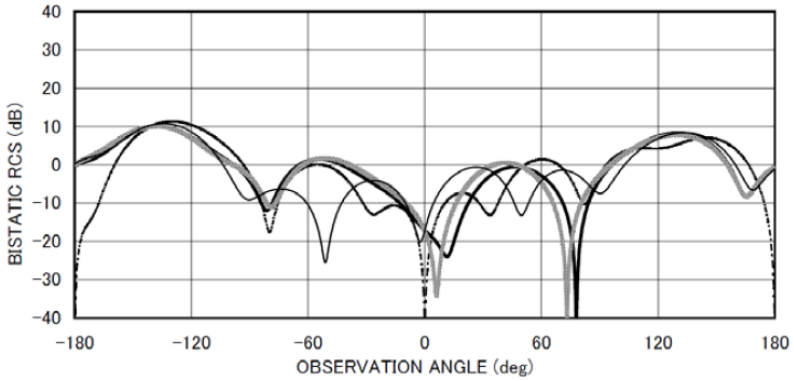

Figure 4a. Bistatic RCS $\sigma/\lambda\,[\mathrm{dB}]$ for $L/b = 1.0, kb = 3.14, \theta_0 = 45°$. -·-·-·-·-·- empty waveguide (layers I-IV: vacuum). ——: cavity with no loading (layer I: perfect conductor; layers II-IV: vacuum; $t_L = 0.6\,L,\ t_{\mathrm{PEC}} = 0.4L,\ t_R = L$). ——: cavity with two-layer loading (layer I: perfect conductor; layer II: $\varepsilon_2 = 3.14{+}i10.0,\ \mu_2 = 1.0$; layer III: $\varepsilon_3 = 1.6{+}i0.9,\ \mu_3 = 1.0$; layer IV: vacuum; $t_L = 0.6L,\ t_{\mathrm{PEC}} = 0.4L,\ t_R = L,\ t_{2\mathrm{layer}} = 0.4L$). ——: cavity with three-layer loading (layer I: perfect conductor; layers II-IV: Emerson & Cuming AN-73; $t_L = 0.6L,\ t_{\mathrm{PEC}} = 0.4L,\ t_R = L,\ t_{3\mathrm{layer}} = 0.6L$).

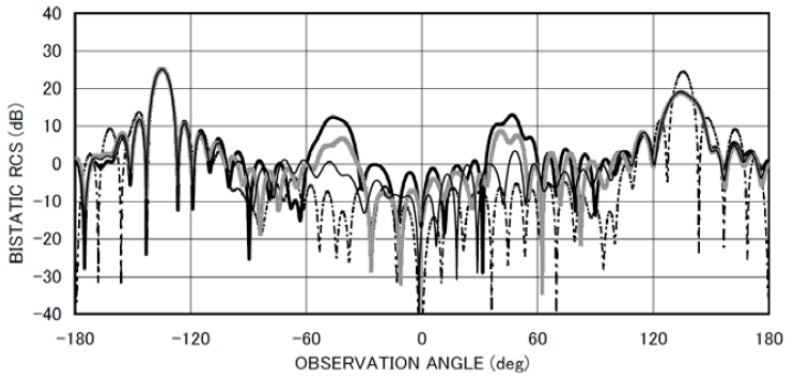

Figure 4b. Bistatic RCS $\sigma/\lambda\,[\mathrm{dB}]$ for $L/b = 1.0,\ kb = 15.7,\ \theta_0 = 45°$. Other particulars are the same as in Fig. 4a.

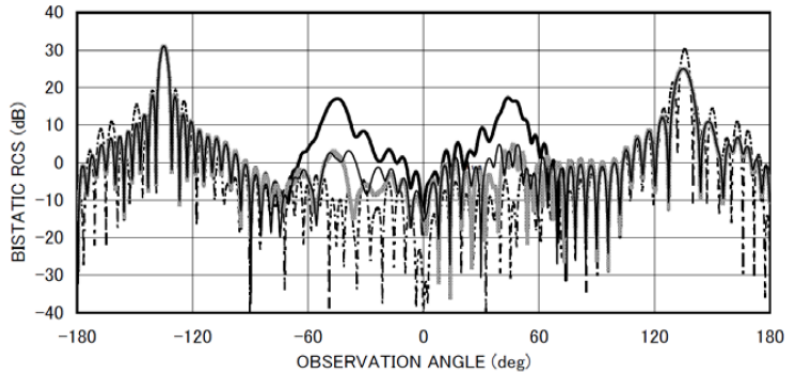

Figure 4c. Bistatic RCS $\sigma/\lambda\,[\mathrm{dB}]$ for $L/b = 1.0,\ kb = 31.4,\ \theta_0 = 45°$. Other particulars are the same as in Fig. 4a.

as $\theta_0 = 45°$ and the other parameters are the same values as in the monostatic RCS. It is seen that in all numerical examples, the bistatic RCS shows sharp peaks at $\theta = -135°$ and $\theta = 135°$, which correspond to the incident and reflected shadow boundaries, respectively. There are also some peaks at $\theta = \pm 45°$ for empty cavities (no material loading in the right cavity) with $kb = 15.7, 31.4$ (Figs. 4(b), 4(c), 5(b), 5(c)), which arise due to the interior irradiation. It is found from these figures that the propagation direction along which the reradiated fields from the cavity are strongly excited depends on the incident angle for large cavity openings.

Next we shall compare the RCS characteristics between the empty

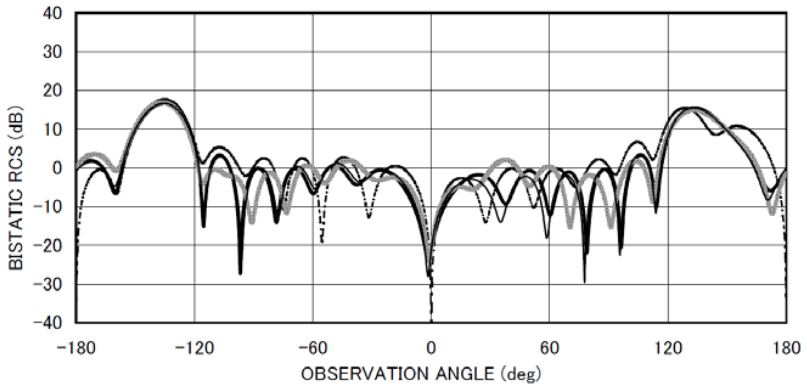

Figure 5a. Bistatic RCS $\sigma/\lambda\,[\mathrm{dB}]$ for $L/b = 3.0, kb = 3.14, \theta_0 = 45°$. Other particulars are the same as in Fig. 4a.

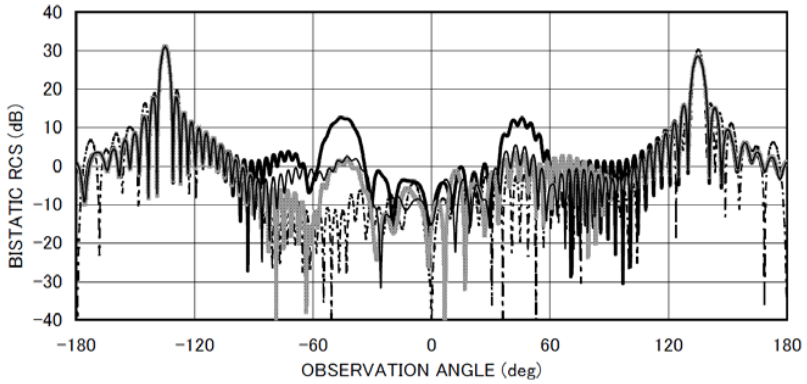

Figure 5b. Bistatic RCS $\sigma/\lambda\,[\mathrm{dB}]$ for $L/b = 3.0, kb = 15.7, \theta_0 = 45°$. Other particulars are the same as in Fig. 4a.

and loaded cavities. On comparing the bistatic RCS data for the empty case (no material loading in the right cavity) with those for the loaded case (material loading in the right cavity), the bistatic RCS for $|\theta| < 60°$ is reduced for the loaded cavities. This is because, the aperture of the right cavity is then visible from observation point and hence, the interior features of the cavity significantly affect the far field bistatic scattering. The RCS reduction for loaded cavities is noticeable for fairly large cavity openings ($kb = 15.7, 31.4$). In addition, it is found that the three-layer material loading leads to a better RCS reduction compared with the two-layer case for large cavities.

It has already been clarified that the monostatic RCS for the two

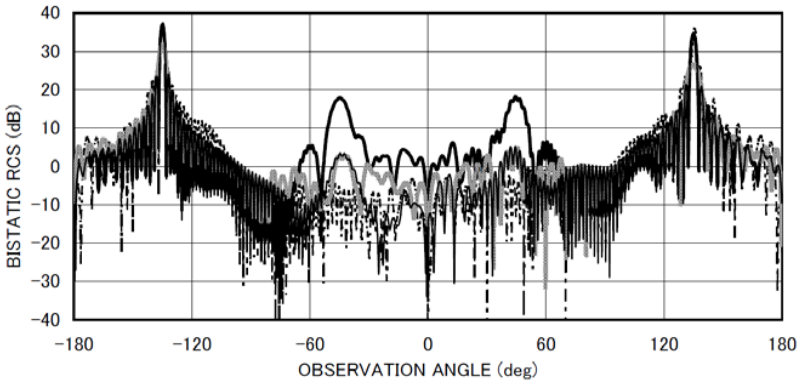

Figure 5c. Bistatic RCS $\sigma/\lambda\,[\mathrm{dB}]$ for $L/b = 3.0, kb = 31.4, \theta_0 = 45°$. Other particulars are the same as in Fig. 4a.

different polarizations shows similar features with an increase of the cavity dimension over the region where the cavity aperture is visible from the indent direction. In the bistatic scattering, however, we find by comparing the results for fairly large cavities in Figs. 4(b), 4(c), 5(b), and 5(c) ($kb = 15.7, 31.4$) for the H-polarized case with the corresponding results for the E-polarized case (Figs. 5(b), 5(c), 6(b), and 6(c) in Part I [21]), there is a difference depending on the incident polarization over a wide range of the observation angle. Hence, it is confirmed that the bistatic RCS characteristics depend on the polarization even at high frequencies.

6. CONCLUSIONS

In this paper, we have considered a finite parallel-plate waveguide with four-layer material loading as a 2-D geometry that can form cavities, and analyzed the H-polarized plane wave diffraction rigorously by means of the Wiener-Hopf technique. We have obtained the solution valid for the waveguide length greater than the incident wavelength. We have carried out numerical computations and given representative numerical examples on the monostatic and bistatic RCS to discuss the scattering characteristics of the waveguide in detail. The final results obtained in this two-part paper for both polarizations are considered as reference solutions and can be used for investigating the range of applicability of other approximate methods.

ACKNOWLEDGMENT

This work was supported in part by the Institute of Science and Engineering, Chuo University.

APPENDIX A. SOME USEFUL FORMULAS FOR THE FOURIER COEFFICIENTS

The Fourier coefficients f_{mn} and g_{mn} for $m = 1, 2, 3, 4, 5$ arising in (25)–(29) are defined as

$$\begin{aligned} f_{mn} &= e^{-\gamma_n(L+D_1)}P_{mn}U_-(-i\gamma_n)+e^{-\gamma_n(L-D_5)}Q_{mn}U_{(+)}(i\gamma_n) \text{ for odd } n, \\ &= -e^{-\gamma_n(L+D_1)}P_{mn}V_-(-i\gamma_n) \\ &\quad +e^{-\gamma_n(L-D_5)}S_{mn}V_{(+)}(i\gamma_n) \quad \text{for even } n, \end{aligned} \tag{A1}$$

$$\begin{aligned} g_{mn} &= e^{-\gamma_n(L+D_1)}R_{mn}U_-(-i\gamma_n) + e^{-\gamma_n(L-D_5)}S_{mn}U_{(+)}(i\gamma_n) \text{ for odd } n, \\ &= -e^{-\gamma_n(L+D_1)}R_{mn}V_-(-i\gamma_n) \\ &\quad +e^{-\gamma_n(L-D_5)}S_{mn}V_{(+)}(i\gamma_n) \text{ for even } n, \end{aligned} \tag{A2}$$

where

$$\begin{aligned} P_{5n} &= (16/G)\varepsilon_2\varepsilon_3\gamma_n\Gamma_{4n}e^{-\Gamma_{4n}(D_5-D_4)} \\ &\quad \cdot e^{-\Gamma_{3n}(D_4-D_3)}e^{-\Gamma_{2n}(D_3-D_2)}e^{-\Gamma_{1n}(D_2-D_1)}, \end{aligned} \tag{A3}$$

$$\begin{aligned} Q_{5n} &= (1/H)\{\mu_4^2\gamma_n\rho_{43n}(\rho_{4n}-1) \\ &\quad +\mu_4\gamma_n[\rho_{43n}\rho_{4n} - e^{-2\Gamma_{4n}(D_5-D_4)}]\}, \end{aligned} \tag{A4}$$

$$\begin{aligned} R_{5n} &= (16/G)\varepsilon_2(\varepsilon_3/\varepsilon_4)\gamma_n\Gamma_{4n}e^{-\Gamma_{4n}(D_5-D_4)} \\ &\quad \cdot e^{-\Gamma_{3n}(D_4-D_3)}e^{-\Gamma_{2n}(D_3-D_2)}e^{-\Gamma_{1n}(D_2-D_1)}, \end{aligned} \tag{A5}$$

$$S_{5n} = -(\varepsilon_4/H)\left[\rho_{43n} - e^{-2\Gamma_{4n}(D_5-D_4)}\right], \tag{A6}$$

$$\begin{aligned} P_{4n} &= (8/G)\varepsilon_2\Gamma_{4n}(\varepsilon_4\gamma_n+\Gamma_{4n})e^{-\Gamma_{3n}(D_4-D_3)} \\ &\quad \cdot e^{-\Gamma_{2n}(D_3-D_2)}e^{-\Gamma_{1n}(D_2-D_1)}\left[e^{-2\Gamma_{4n}(D_5-D_4)}+\rho_{4n}\right], \end{aligned} \tag{A7}$$

$$\begin{aligned} Q_{4n} &= -\frac{1}{H}\left[\frac{\varepsilon_4}{\varepsilon_3}\Gamma_{4n}(\rho_{43n}+\varepsilon_4)e^{-\Gamma_{4n}(D_5-D_4)}\right. \\ &\quad \left.-\varepsilon_4\rho_{43n}(\rho_{4n}+1)\left(\gamma_n\frac{\varepsilon_4^2}{2\varepsilon_3}\delta_{4n}+\Gamma_{4n}\right)e^{\Gamma_{4n}(D_5-D_4)}\right], \end{aligned} \tag{A8}$$

$$R_{4n} = (1/G)\left[(8\varepsilon_2\varepsilon_3/\varepsilon_4)(\varepsilon_4\gamma_n + \Gamma_{4n})e^{-\Gamma_{3n}(D_4-D_3)}\right.$$
$$\left.\cdot e^{-\Gamma_{2n}(D_3-D_2)}e^{-\Gamma_{1n}(D_2-D_1)}\left(e^{-2\Gamma_{4n}(D_5-D_4)} - \rho_{4n}\right)\right], \quad \text{(A9)}$$

$$S_{4n} = \frac{1}{H}\left[\varepsilon_4(\rho_{43n}-1)e^{-\Gamma_{4n}(D_5-D_4)} - \frac{\varepsilon_4}{2}\,\rho_{43n}(\rho_{4n}+1)\right.$$
$$\left.\cdot\left(\frac{\gamma_n}{\Gamma_{4n}}\varepsilon_4\delta_{4n}+1\right)e^{\Gamma_{4n}(D_5-D_4)}\right], \quad \text{(A10)}$$

$$P_{3n} = \frac{1}{G}\frac{4\varepsilon_2^2}{\varepsilon_3\varepsilon_4}\left(\varepsilon_4\gamma_n + \Gamma_{4n}\right)\left(\frac{\Gamma_{3n}\varepsilon_3}{\varepsilon_4} + \Gamma_{4n}\right)e^{-\Gamma_{2n}(D_3-D_2)}$$
$$\cdot e^{-\Gamma_{1n}(D_2-D_1)}\left\{e^{-2\Gamma_{4n}(D_5-D_4)}\left[e^{-2\Gamma_{3n}(D_4-D_3)} + \rho_{3n}\right]\right.$$
$$\left.+\rho_{4n}\rho_{3n}\left[e^{-2\Gamma_{3n}(D_4-D_3)}+1\right]\right\}, \quad \text{(A11)}$$

$$Q_{3n} = \frac{1}{H}\left\{\frac{\varepsilon_2 I}{2\varepsilon_3}e^{-\Gamma_{4n}(D_5-D_4)}\left[x_{3n}e^{-\Gamma_{3n}(D_4-D_3)} - e^{\Gamma_{3n}(D_4-D_3)}\right]\right.$$
$$\left.+\frac{\varepsilon_2 J}{2\varepsilon_3 s}\rho_{4n+1}e^{\Gamma_{4n}(D_5-D_4)}\left[y_{3n}e^{-\Gamma_{3n}(D_4-D_3)} + e^{\Gamma_{3n}(D_4-D_3)}\right]\right\}, \quad \text{(A12)}$$

$$R_{3n} = (1/G)\left((4\varepsilon_2/\Gamma_{3n})\left(\varepsilon_4\gamma_n + \Gamma_4 n\right)\left[(\varepsilon_3\Gamma_3 n/\varepsilon_4) + \Gamma_4 n\right]\right.$$
$$\cdot e^{-\Gamma_{2n}(D_3-D_2)}e^{-\Gamma_{1n}(D_2-D_1)}\left\{e^{-2\Gamma_4 n(D_5-D_4)}\right.$$
$$\left.\left.\cdot\left[e^{-2\Gamma_{3n}(D_4-D_3)} - \rho_{3n}\right] + \rho_{4n}\left[\rho_{3n}e^{-2\Gamma_{2n}(D_4-D_3)} - 1\right]\right\}\right), \quad \text{(A13)}$$

$$S_{3n} = \frac{1}{H}\left\{\frac{I}{2\Gamma_{3n}}e^{\Gamma_{4n}(D_5-D_4)}\left[x_{3n}e^{-\Gamma_{3n}(D_4-D_3)} + e^{\Gamma_{3n}(D_4-D_3)}\right]\right.$$
$$+\frac{J}{2\Gamma_{3n}}\left(\rho_{4n}+1\right)e^{\Gamma_{4n}(D_5-D_4)}$$
$$\left.\left[y_{3n}e^{-\Gamma_{3n}(D_4-D_3)} - e^{-\Gamma_{3n}(D_4-D_3)}\right]\right\}, \quad \text{(A14)}$$

$$P_{2n} = \frac{2\varepsilon_2}{G}\left(\varepsilon_4\gamma_n + \Gamma_{4n}\right)\left(\frac{\varepsilon_3\Gamma_{3n}}{\varepsilon_4} + \Gamma_{4n}\right)(R_1 + R_2), \quad \text{(A15)}$$

$$Q_{2n} = (1/4H)(R_3 + R_4), \quad \text{(A16)}$$

$$R_{2n} = \frac{2\varepsilon_2}{G}(\varepsilon_4\gamma_n + \Gamma_{4n})\left(\frac{\varepsilon_3\Gamma_{3n}}{\varepsilon_4} + \Gamma_{4n}\right)e^{-\Gamma_{1n}(D_2-D_1)}(S_1+S_2), \quad \text{(A17)}$$

$$S_{2n} = (1/4H)(S_3 + S_4), \quad \text{(A18)}$$

$$P_{1n} = \frac{1}{G}\left\{(\varepsilon_4\gamma_n + \Gamma_{4n})\left(\frac{\varepsilon_3\Gamma_{3n}}{\varepsilon_4} + \Gamma_{4n}\right)\right.$$
$$\cdot R_1\left(\varepsilon_1 + \frac{\varepsilon_2\Gamma_{3n}}{\Gamma_{2n}}\xi_{1n}\right)\left[e^{-2\Gamma_{1n}(D_2-D_1)} + \omega_{1n}\right]$$
$$\left. + R_2\left(\varepsilon_1 + \frac{\varepsilon_2\Gamma_{3n}}{\Gamma_{2n}}\xi_{1n}{}'\right)\left[e^{-2\Gamma_{bn}(D_2-D_1)} + \omega'_{1n}\right]\right\}, \tag{A19}$$

$$Q_{1n} = \frac{1}{H}\left\{R_3\left(\frac{\varepsilon_1}{2\varepsilon_2} + \frac{\Gamma_{1n}}{2\Gamma_{2n}}\tau_{1n}\right)\left[e^{-\Gamma_{1n}(D_2-D_1)} + e^{\Gamma_{1n}(D_2-D_1)\tau_{1n}}\right]\right.$$
$$\left. + R_4\left(\frac{\varepsilon_1}{2\varepsilon_2} + \frac{\Gamma_{1n}}{2\Gamma_{2n}}\tau'_{1n}\right)\left[e^{-\Gamma_{1n}(D_2-D_1)} + e^{\Gamma_{1n}(D_2-D_1)\tau'_{1n}}\right]\right\}, \tag{A20}$$

$$R_{1n} = \frac{1}{G}\left\{\frac{S_1}{2\Gamma_{1n}}(\varepsilon_4\gamma_n + \Gamma_{4n})\left(\frac{\varepsilon_3\Gamma_{3n}}{\varepsilon_4} + \Gamma_{4n}\right)\right.$$
$$\cdot\left(\varepsilon_1 + \frac{\varepsilon_3\Gamma_{3n}}{\varepsilon_2}\xi_{1n}\right)\left[e^{-2\Gamma_{1n}(D_2-D_1)} - \omega_{1n}\right]$$
$$\left. + S_2\left(\varepsilon_1 + \frac{\varepsilon_3\Gamma_{3n}}{\varepsilon_2}\xi'_{1n}\right)\left[e^{-2\Gamma_{1n}(D_2-D_1)} - \omega'_{1n}\right]\right\}, \tag{A21}$$

$$S_{1n} = \frac{1}{4H}\left\{S_3\left(\frac{\varepsilon_1}{\varepsilon_2} + \frac{\tau_{1n}\Gamma_{1n}}{\Gamma_{2n}}\right)\left[e^{-\Gamma_{1n}(D_2-D_1)} + e^{\Gamma_{1n}(D_2-D_1)}\tau_{1n}\right]\right.$$
$$\left. + S_4\left(\frac{\varepsilon_1}{\varepsilon_2} + \frac{\tau'_{1n}\Gamma_{1n}}{\Gamma_{2n}}\right)\left[e^{-\Gamma_{1n}(D_2-D_1)} + e^{\Gamma_{1n}(D_2-D_1)}\tau'_{1n}\right]\right\}, \tag{A22}$$

$$G = (\varepsilon_1\gamma_n + \Gamma_{1n})(\varepsilon_4\gamma_n + \Gamma_{1n})\left(\frac{\varepsilon_3}{\varepsilon_4} + \frac{\delta_{32n}\Gamma_{4n}}{\Gamma_{3n}}\right)\left(\frac{\varepsilon_2}{\varepsilon_1} + \frac{\delta_{1n}\Gamma_{2n}}{\Gamma_{1n}}\right)$$
$$\cdot\left[\rho_{43n}\rho_{4n} - e^{-2\Gamma_{4n}(D_5-D_4)}\right]\left[\rho_{32n} + e^{-2\Gamma_{3n}(D_4-D_3)}\right]$$
$$\cdot\left[\rho_{21n} + e^{-2\Gamma_{2n}(D_3-D_2)}\right]\left[1 + e^{-2\Gamma_{1n}(D_2-D_1)}\rho_{1n}\right], \tag{A23}$$

$$H = (\varepsilon_4\gamma_{4n} + \Gamma_{4n})\left[\rho_{43n}\rho_{4n} - e^{-2\Gamma_{4n}(D_5-D_4)}\right], \tag{A24}$$

$$I = \left[\varepsilon_4\Gamma_{3n}(\rho_{43n} - 1) + \Gamma_{4n}(\varepsilon_4/\varepsilon_3)(\rho_{4n} + \varepsilon_4)\right]^{-1}, \tag{A25}$$

$$J = \left[\varepsilon_4\rho_{43n}\left(\frac{\varepsilon_4^2\delta_{4n}\gamma_n}{2\varepsilon_3} + \Gamma_{4n}\right) + \frac{\varepsilon_4}{2}\Gamma_{3n}\rho_{43n}\left(\frac{\varepsilon_4\delta_{4n}\gamma_n}{\Gamma_{4n}} + 1\right)\right]^{-1}, \tag{A26}$$

$$R_1 = e^{-\Gamma_{4n}(D_5-D_4)}\left[e^{-\Gamma_{3n}(D_4-D_3)} + \rho_{3n}\right]$$
$$\cdot\left(\frac{\varepsilon_1}{\varepsilon_2} + \frac{\delta'_{32}\Gamma_{2n}}{\Gamma_{3n}}\right)\left[e^{-2\Gamma_{2n}(D_3-D_2)} + \xi_{2n}\right], \tag{A27}$$

$$R_2 = \rho_{4n}\left[e^{-2\Gamma_{3n}(D_4-D_3)}\rho_{3n}+1\right] \cdot\left(\frac{\varepsilon_1}{\varepsilon_2}+\frac{\delta'_{32n}\Gamma_{2n}}{\Gamma_{3n}}\right)\left[e^{-2\Gamma_{2n}(D_3-D_2)}+\xi'_{32n}\right], \tag{A28}$$

$$R_3 = Ie^{-\Gamma_{4n}(D_5-D_4)}\left[e^{-\Gamma_{3n}(D_4-D_3)}+e^{\Gamma_{3n}(D_4-D_3)}\right]x_{3n} \cdot\left(\frac{\varepsilon_2 x_{2n}}{\varepsilon_3}+\frac{\Gamma_{2n}}{\Gamma_{3n}}\right)\left[e^{-\Gamma_{2n}(D_3-D_2)}+e^{\Gamma_{2n}(D_3-D_2)}\tau_{2n}\right], \tag{A29}$$

$$R_4 = J\left(\rho_{4n}+1\right)e^{-\Gamma_{4n}(D_5-D_4)}\left[e^{-\Gamma_{3n}(D_4-D_3)}+e^{\Gamma_{3n}(D_4-D_3)}\right]y_{3n} \cdot\left(\frac{\varepsilon_2}{\varepsilon_3}+\frac{\Gamma_{2n}y_{2n}}{\Gamma_{3n}}\right)\left[e^{-\Gamma_{2n}(D_3-D_2)}+e^{\Gamma_{2n}(D_3-D_2)}\tau'_{2n}\right], \tag{A30}$$

$$S_1 = e^{-2\Gamma_{4n}(D_5-D_4)}\left[e^{-2\Gamma_{3n}(D_4-D_3)}+\rho_{3n}\right] \cdot\left(\frac{\varepsilon_1}{\varepsilon_2}+\frac{\delta_{32n}\Gamma_{2n}}{\Gamma_{3n}}\right)\left[e^{-\Gamma_{2n}(D_3-D_2)}+\xi_{2n}\right], \tag{A31}$$

$$S_2 = \rho_{4n}\left[e^{-2\Gamma_{3n}(D_4-D_3)}\rho_{3n}+1\right] \cdot\left(\frac{\varepsilon_2}{\varepsilon_3}+\frac{\delta'_{32n}\Gamma_{2n}}{\Gamma_{3n}}\right)\left[e^{-2\Gamma_{2n}(D_3-D_2)}-\xi'_{32n}\right], \tag{A32}$$

$$S_3 = (I/\Gamma_{2n})e^{-\Gamma_{4n}(D_5-D_4)}\left[x_{3n}e^{-\Gamma_{3n}(D_4-D_3)}+e^{\Gamma_{3n}(D_4-D_3)}\right] \cdot\left(\frac{\varepsilon_2 x_{2n}}{\varepsilon_3}+\frac{\Gamma_{4n}}{\Gamma_{3n}}\right)\left[e^{-\Gamma_{2n}(D_3-D_2)}-e^{\Gamma_{2n}(D_3-D_2)}\tau_{2n}\right], \tag{A33}$$

$$S_4 = (J/\Gamma_{2n})\left(\rho_{4n}+1\right)e^{\Gamma_{4n}(D_5-D_4)}\left[y_{3n}e^{-\Gamma_{3n}(D_4-D_3)}+e^{\Gamma_{3n}(D_4-D_3)}\right] \cdot\left(\frac{\varepsilon_2}{\varepsilon_3}+\frac{\Gamma_{4n}y_{2n}}{\Gamma_{3n}}\right)\left[e^{-\Gamma_{2n}(D_3-D_2)}-e^{\Gamma_{2n}(D_3-D_2)}\tau'_{2n}\right], \tag{A34}$$

$$x_{3n} = \frac{\varepsilon_3\varepsilon_4\Gamma_{4n}(\rho_{43n}-1)-\varepsilon_4\Gamma_{3n}(\rho_{4n}+\varepsilon_4)}{\varepsilon_3\varepsilon_4\Gamma_{4n}(\rho_{43n}-1)+\varepsilon_4\Gamma_{3n}(\rho_{4n}+\varepsilon_4)}, \tag{A35}$$

$$y_{3n} = \frac{\varepsilon_4\rho_{43n}\left(\gamma_n\varepsilon_4^2\delta_{4n}/\varepsilon_3+2\Gamma_{4n}\right)-\varepsilon_4\Gamma_{3n}\rho_{43n}\left(\gamma_n\varepsilon_4\delta_{4n}/\Gamma_{4n}+1\right)}{\varepsilon_4\rho_{43n}\left(\gamma_n\varepsilon_4^2\delta_{4n}/\varepsilon_3+2\Gamma_{4n}\right)+\varepsilon_4\Gamma_{3n}\rho_{43n}\left(\gamma_n\varepsilon_4\delta_{4n}/\Gamma_{4n}+1\right)}, \tag{A36}$$

$$x_{2n} = \frac{x_{3n}e^{-\Gamma_{3n}(D_4-D_3)}-e^{-\Gamma_{3n}(D_4-D_3)}}{x_{3n}e^{-\Gamma_{3n}(D_4-D_3)}+e^{-\Gamma_{3n}(D_4-D_3)}}, \tag{A37}$$

$$y_{2n} = \frac{y_{3n}e^{-\Gamma_{3n}(D_4-D_3)}-e^{-\Gamma_{3n}(D_4-D_3)}}{y_{3n}e^{-\Gamma_{3n}(D_4-D_3)}+e^{-\Gamma_{3n}(D_4-D_3)}}, \tag{A38}$$

$$\rho_{43n} = \frac{\varepsilon_3\Gamma_{3n}-\delta_{32n}\varepsilon_4\Gamma_{4n}}{\varepsilon_3\Gamma_{3n}+\delta_{32n}\varepsilon_4\Gamma_{4n}}, \rho_{32n} = \frac{\varepsilon_3\Gamma_{2n}-\delta_{21n}\varepsilon_2\Gamma_{3n}}{\varepsilon_3\Gamma_{2n}+\delta_{21n}\varepsilon_2\Gamma_{3n}}, \tag{A39}$$

$$\rho_{21n}=\frac{\varepsilon_1\Gamma_{1n}-\delta_{21n}\varepsilon_2\Gamma_{2n}}{\varepsilon_1\Gamma_{1n}+\delta_{21n}\varepsilon_2\Gamma_{2n}},\ \rho_{4n}=\frac{\varepsilon_4\gamma_n-\Gamma_{4n}}{\varepsilon_4\gamma_n+\Gamma_{4n}}, \tag{A40}$$

$$\rho_{3n}=\frac{\varepsilon_4\Gamma_{4n}-\varepsilon_3\Gamma_{3n}}{\varepsilon_4\Gamma_{4n}+\varepsilon_3\Gamma_{3n}},\rho_{1n}=\frac{\varepsilon_1\gamma_n-\Gamma_{1n}}{\varepsilon_1\gamma_n+\Gamma_{1n}}, \tag{A41}$$

$$\delta_{32n}=\frac{e^{-2\Gamma_{3n}(D_4-D_3)}-\rho_{32n}}{e^{-2\Gamma_{3n}(D_4-D_3)}+\rho_{32n}},\delta_{21n}=\frac{e^{-2\Gamma_{2n}(D_3-D_2)}-\rho_{21n}}{e^{-2\Gamma_{2n}(D_3-D_2)}+\rho_{21n}}, \tag{A42}$$

$$\delta_{1n}=\frac{e^{-2\Gamma_{1n}(D_2-D_1)}-\rho_{1n}}{e^{-2\Gamma_{1n}(D_2-D_1)}+\rho_{1n}},\delta'_{32n}=\frac{e^{-2\Gamma_{3n}(D_3-D_2)}\rho_{3n}-1}{e^{-2\Gamma_{3n}(D_4-D_3)}\rho_{3n}+1}, \tag{A43}$$

$$\delta_{4n}=(\rho_{4n}-1)/(\rho_{4n}+1), \tag{A44}$$

$$\xi_{2n}=\frac{\varepsilon_2\Gamma_{3n}-\varepsilon_3\Gamma_{2n}\delta_{32n}}{\varepsilon_2\Gamma_{3n}+\varepsilon_3\Gamma_{2n}\delta_{32n}},\xi'_{2n}=\frac{\varepsilon_2\Gamma_{3n}-\varepsilon_3\Gamma_{2n}\delta'_{32n}}{\varepsilon_2\Gamma_{3n}+\varepsilon_3\Gamma_{2n}\delta'_{32n}}, \tag{A45}$$

$$\xi_{1n}=\frac{e^{-2\Gamma_{2n}(D_3-D_2)}-\xi_{2n}}{e^{-2\Gamma_{2n}(D_3-D_2)}+\xi_{2n}},\xi'_{1n}=\frac{e^{-2\Gamma_{2n}(D_3-D_2)}-\xi'_{2n}}{e^{-2\Gamma_{2n}(D_3-D_2)}+\xi'_{2n}}, \tag{A46}$$

$$\tau_{2n}=\frac{\varepsilon_2x_{2n}\Gamma_{3n}-\varepsilon_3\Gamma_{2n}}{\varepsilon_2x_{2n}\Gamma_{3n}+\varepsilon_3\Gamma_{2n}},\tau'_{2n}=\frac{\varepsilon_2\Gamma_{3n}-\varepsilon_3y_{2n}\Gamma_{2n}}{\varepsilon_2\Gamma_{3n}+\varepsilon_3y_{2n}\Gamma_{2n}}, \tag{A47}$$

$$\tau_{1n}=\frac{e^{-\Gamma_{2n}(D_3-D_2)}-e^{-2\Gamma_{2n}(D_3-D_2)}\tau_{2n}}{e^{-\Gamma_{2n}(D_3-D_2)}+e^{-2\Gamma_{2n}(D_3-D_2)}\tau_{2n}},$$

$$\tau'_{1n}=\frac{e^{-\Gamma_{2n}(D_3-D_2)}-e^{-2\Gamma_{2n}(D_3-D_2)}\tau'_{2n}}{e^{-\Gamma_{2n}(D_3-D_2)}+e^{-2\Gamma_{2n}(D_3-D_2)}\tau'_{2n}}, \tag{A48}$$

$$\omega_{1n}=\frac{\varepsilon_1\Gamma_{2n}-\varepsilon_2\Gamma_{3n}\xi_{1n}}{\varepsilon_1\Gamma_{2n}+\varepsilon_2\Gamma_{3n}\xi_{1n}},\omega'_{1n}=\frac{\varepsilon_1\Gamma_{2n}-\varepsilon_2\Gamma_{3n}\xi'_{1n}}{\varepsilon_1\Gamma_{2n}+\varepsilon_2\Gamma_{3n}\xi'_{1n}}, \tag{A49}$$

REFERENCES

1. Lee, S.-W. and H. Ling, "Data book for cavity RCS: Version 1," *Tech. Rep.*, No. SWL 89-1, Univ. Illinois, Urbana, 1989.
2. Lee, S.-W. and R. J. Marhefka, "Data book of high-frequency RCS: Version 2," *Tech. Rep.*, Univ. Illinois, Urbana, 1989.
3. Stone, W. R. (ed.), *Radar Cross Sections of Complex Objects*, IEEE Press, New York, 1990.
4. Bernard, J. M. L., G. Pelosi, and P. Ya. Ufimtsev (eds.), *Special Issue on Radar Cross Section of Complex Objects, Ann. Telecommun.*, Vol. 50, No. 5–6, 1995.
5. Lee, C. S. and S.-W. Lee, "RCS of coated circular waveguide terminated by a perfect conductor," *IEEE Trans. Antennas Propagat.*, Vol. 35, No. 4, 391–398, 1987.
6. Altintaş, A., P. H. Pathak, and M. C. Liang, "A selective modal

scheme for the analysis of EM coupling into or radiation from large open-ended waveguides," *IEEE Trans. Antennas Propagat.*, Vol. 36, No. 1, 84–96, 1988.

7. Ling, H., R.-C. Chou, and S.-W. Lee, "Shooting and bouncing rays: Calculating the RCS of an arbitrary shaped cavity," *IEEE Trans. Antennas Propagat.*, Vol. 37, No. 2, 194–205, 1989.
8. Pathak, P. H. and R. J. Burkholder, "Moday, ray, and beam techniques for analyzing the EM scattering by open-ended waveguide cavities," *IEEE Trans. Antennas Propagat.*, Vol. 37, No. 5, 635–647, 1989.
9. Pathak, P. H. and R. J. Burkholder, "A reciprocity formulation for the EM scattering by an obstacle within a large open cavity," *IEEE Trans. Microwave Theory Tech.*, Vol. 41, No. 4, 702–707, 1993.
10. Lee, R. and T.-T. Chia, "Analysis of electromagnetic scattering from a cavity with a complex termination by means of a hybrid ray-FDTD method," *IEEE Trans. Antennas Propagat.*, Vol. 41, No. 11, 1560–1569, 1993.
11. Ohnuki, S. and T. Hinata, "Radar cross section of an open-ended rectangular cylinder with an iris inside the cavity," *IEICE Trans. Electron.*, Vol. E81-C, No. 12, 1875–1880, 1998.
12. Büyükaksoy, A., F. Birbir, and E. Erdoğan, "Scattering characteristics of a rectangular groove in a reactive surface," *IEEE Trans. Antennas and Propagat.*, Vol. 43, No. 12, 1450–1458, 1995.
13. Çetiner, B. A., A. Büyükaksoy, and F. Güneş, "Diffraction of electromagnetic waves by an open ended parallel plate waveguide cavity with impedance walls," *Progress In Electromagnetics Research*, PIER 26, 165–197, 2000.
14. Kobayashi, K. and A. Sawai, "Plane wave diffraction by an open-ended parallel plate waveguide cavity," *Journal of Electromagnetic Waves and Applications*, Vol. 6, No. 4, 475–512, 1992.
15. Koshikawa, S., T. Momose, and K. Kobayashi, "RCS of a parallel-plate waveguide cavity with three-layer material loading," *IEICE Trans. Electron.*, Vol. E77-C, No. 9, 1514–1521, 1994.
16. Koshikawa, S. and K. Kobayashi, "Diffraction by a terminated, semi-infinite parallel-plate waveguide with three-layer material loading," *IEEE Trans. Antennas and Propagat.*, Vol. 45, No. 6, 949–959, 1997.
17. Koshikawa, S. and K. Kobayashi, "Diffraction by a terminated, semi-infinite parallel-plate waveguide with three-layer material loading: the case of H polarization," *Electromagnetic Waves &*

Electronic Systems, Vol. 5, No. 1, 13–23, 2000.

18. Kobayashi, K. and S. Koshikawa, "Wiener-Hopf analysis of the radar cross section of parallel-plate waveguide cavities," *Tech. Rep.*, No. KK96-3-8, Chuo Univ., Tokyo, 1996.
19. Okada, S., S. Koshikawa, and K. Kobayashi, "Wiener-Hopf analysis of the plane wave diffraction by a finite parallel-plate waveguide with three-layer material loading: Part I: The case of E polarization," *Telecommunications and Radio Engineering*, Vol. 58, No. 1–2, 53–65, 2002.
20. Okada, S., S. Koshikawa, and K. Kobayashi, "Wiener-Hopf analysis of the plane wave diffraction by a finite parallel-plate waveguide with three-layer material loading: Part II: The case of H polarization," *Telecommunications and Radio Engineering*, Vol. 58, No. 1–2, 66–75, 2002.
21. Zheng, J. P. and K. Kobayashi, "Plane wave diffraction by a finite parallel-plate waveguide with four-layer material loading: Part I — The case of E polarization," *Progress In Electromagnetics Research B*, Vol. 6, 1–36, 2008.
22. Kobayashi, K., "On generalized gamma functions occurring in diffraction theory," *J. Phys. Soc. Japan*, Vol. 60, No. 5, 1501–1512, 1991.